Fusion Engineering and Design 216 (2025) 115065

Contents lists available at ScienceDirect

Fusion Engineering and Design

journal homepage: www.elsevier.com/locate/fusengdes

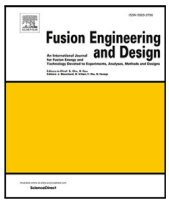

Fins: Improving tritium extraction systems and permeation sensors with the adoption of extended surfaces

Ciro Alberghi [a],*, Luigi Candido [b], Daniele Martelli [a], Francesca Papa [a], Marco Utili [a], Alessandro Venturini [a]

[a] ENEA C.R. Brasimone – Località Brasimone, 40043 Camugnano (BO), Italy
[b] Kyoto Fusioneering UK Ltd, 200 Brook Drive RG26UB Reading, UK

ARTICLE INFO

Keywords:
Hydrogen isotopes
Permeation
Tritium extraction
PAV
Optimisation

ABSTRACT

Tritium extraction from lithium-lead (PbLi, 15.7 at. % Li) and tritium concentration measurement in the eutectic alloy represent some of the most challenging aspects of the R&D activities aimed to the development of ITER and the European DEMO reactor. To efficiently design Permeator Against Vacuum (PAV) systems and Hydrogen isotopes Permeation Sensors (HPS), theoretical models for the evaluation of the permeation flux have been proposed in literature, but methodologies for the improvement of their performances are still lacking. In this paper a new concept of finned permeator is analysed, leveraging the analogy between mass transport and heat transfer. In PAV and HPS, the low-pressure side is usually kept under medium/high vacuum conditions and surface phenomena can play an important role, especially when the membrane presents oxidation. The fin approach is particularly effective in these cases, where transport kinetics is dominated by surface effects (diffusion in the bulk is relatively fast) and can be used as a method to increase the permeation of hydrogen isotopes with limited increase in system size. Within the paper, the mathematical model for the extended surface placed on the vacuum side is derived and simple relations for design parameters for the finned surface, like fin efficiency and effectiveness, are derived. The solution of this analytical model is compared with numerical results for a PAV system with niobium membrane under relevant conditions for DEMO reactor.

1. Introduction

Over the last two decades, there has been a surge of interest in developing technologies for measuring and extracting tritium from liquid PbLi. For example, ENEA C. R. Brasimone, in collaboration with Politecnico di Torino, has developed hydrogen isotopes Permeation Sensors (HPS) based on pure α-iron membranes since the 2000s [1–4]; these sensors have been characterised under both static and flowing PbLi conditions [5]. As for the tritium extraction technologies, several liquid metal loops have been developed and operated [6–9], and different hydrogen isotopes extraction systems have been studied and characterised, such as the Gas–Liquid Contactor (GLC), the Permeator Against Vacuum (PAV) [10–16] and the Liquid-Vacuum Contactor (LVC) with Vacuum Sieve Tray (VST) [17] or Free Surface configurations [18]. Among these, the PAV concept should be highlighted as it is the reference technology envisaged for the European reactor DEMO [19] where the reference design adopts niobium U-tubes [20].

As far as modelling is concerned, most analytical models have been developed for gas-driven permeation [21–23]. In general, the permeation of hydrogen isotopes is influenced by multiple factors: surface adsorption and desorption, surface to bulk migration, bulk diffusivity and solubility, and hydrogen-defects interactions. Neglecting the presence of structure defects or trapping sites and assuming surface–subsurface equilibrium [22], one can identify two limiting regimes: the diffusion-limited regime (DLR) and the surface-limited regime (SLR) [21]. However, if the upstream side is PbLi (or more generally a liquid metal), the hydrogen isotopes are monoatomically dissolved in the liquid. To account for transport into the liquid phase, a mass transfer coefficient is usually assumed in this framework. In 2015, Humrickhouse and Merril [24] have developed an analytical model that takes into account the mass transfer coefficient of tritium in PbLi assuming a DLR. However, this assumption does not always hold, especially for permeators based on V-group metals (like niobium), as surface effects can play a major role. In 2022, the model was extended including surface effects by [25].

When surface effects are non-negligible, tritium permeation can be improved exploiting a strategy widely used in heat transfer systems. Heat and mass transfer have analogous mathematical descriptions, although the quantities and boundary conditions involved are different. In heat exchanger design, it is common practise to introduce

* Corresponding author.
E-mail address: ciro.alberghi@enea.it (C. Alberghi).

https://doi.org/10.1016/j.fusengdes.2025.115065
Received 10 January 2025; Received in revised form 12 March 2025; Accepted 7 April 2025
Available online 24 April 2025

Table 1
Summary of the variables introduced in Section 2. Superscript * indicates the dimensionless variable.

Name	Symbol	Definition	Unit
Fin length	l	–	m
Fin thickness	δ, δ^*	–, $\frac{\delta}{l}$	m, –
Fin width	w	–	m
Fin perimeter	P	$2(w+\delta)$	m
Fin lateral area	A_l	Pl	m^2
Fin cross-section	A_c	$w\delta$	m^2
Primary membrane thickness	t, t^*	–, $\frac{t}{l}$	m, –
Primary membrane height	H	–	m
Permeation rate	ϕ	–	mol s^{-1}
Diffusivity	D	–	m^2 s^{-1}
Recombination coefficient	K_r	–	m^4 mol^{-1} s^{-1}
Sieverts' constant	K_s	–	mol m^{-3} $Pa^{-\frac{1}{2}}$
Hydrogen isotope partial pressure	p	–	Pa
Hydrogen isotope concentration	c, c^*	–, $\frac{c}{K_{s,s}\sqrt{p}}$	mol m^{-3}, –
Permeation parameter	W	$\frac{K_r K_{s,s} t \sqrt{p}}{D}$	–
Fin parameter	W_f	$\frac{2Wl^2}{\delta t}$	–
Fin efficiency	η_f	Eq. (17)	–
Fin effectiveness	ϵ_f	Eq. (24)	–
Overall effectiveness	ϵ_o	Eq. (30)	–

secondary/extended surfaces (fins) when the convective heat removal of the system is poor. In the current heat and mass transfer analogy, the heat removed by convection is analogous to the release of chemical species from the surface. It will be shown in the article that the use of secondary surfaces on the vacuum side can be advantageous for permeators if transport kinetics are limited by surface effects e.g. when the surface is affected by impurities, for high permeable membranes and/or when very small driving hydrogen pressure are considered. According to theoretical results, secondary surfaces lead to an increase in permeation area in surface-limited or surface-dominant regimes. They can increase the permeation rate per unit height of the system and thus improve system performance and reduce the size of the component. In this context, the fin approach can be used for systems where hydrogen isotopes need to be extracted (PAV) or measured (HPS) without any relevant drawbacks related to the presence of secondary surfaces. A mathematical description of the analytical model based on the fin approach can be found in Section 2. Important design parameters of the finned system, fin efficiency and effectiveness, will be derived. An example of an application for a PAV system considering relevant tritium transport conditions for fusion application is described in Section 3.

2. Mathematical model of transport through the extended surface

The detailed description of the rate equations behind hydrogen isotope transport in a PAV system can be found in [25]. As reported, the concentration gradient of the hydrogen isotope in the solid membrane is small or close to zero in the surface-dominating and surface limited regimes. Under these conditions, secondary surfaces (fins) connected to the membrane, referred to as the primary surface, placed on the vacuum side, lead to an increase in permeation area and can thus increase the permeation rate per unit height of the system. This results in an improvement of the system performance and a reduction in the size of the component.

In the next subsections, the mathematical model describing the transport in the secondary surfaces is derived and performance parameters useful for the design of finned systems are defined. The summary of all the variables introduced in the next subsections is reported in Table 1.

2.1. Mathematical model

Consider a fin of thickness δ (m), total length l (m) and width w (m) connected to a primary surface of thickness t (m), and shown in Fig. 1.

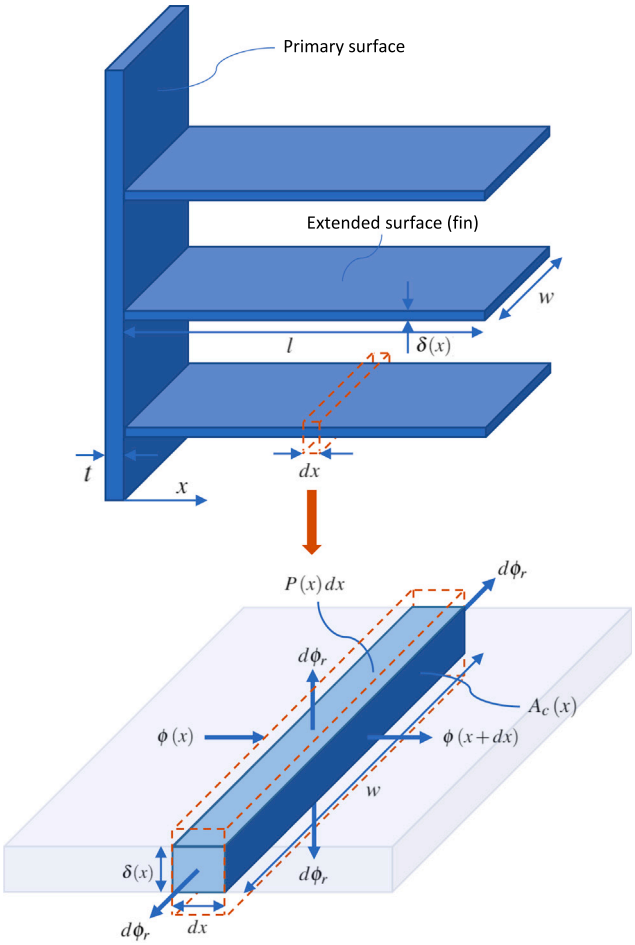

Fig. 1. *Top:* Primary and extended surfaces representation. The secondary surface is placed on the vacuum side. *Bottom:* Model representation. Permeation flux contributions on the differential element of the fin. In light blue the lateral surface $P(x)$ of the element, in dark blue the cross-sectional area A_c.

The thickness δ can generally vary with x, so also the lateral area $A_l(x) = 2\int_0^l (w+\delta(x))dx$ (m^2) and the cross-sectional area $A_c(x) = w\delta(x)$ (m^2). If δ is constant, $A_l = 2l(w+\delta)$ and $A_c = w\delta$. The following assumptions are considered in the analysis:

- Transport of single species;
- Steady state analysis;
- HIs release from surface based on Waelbroeck assumption [22] and Pick and Sonnenberg recombination coefficient [23];
- Constant and uniform properties of the material;
- Negligible pressure of the vacuum side, thus the incoming dissociation flux is not included;
- Thin fin ($\delta \ll l \ll w$), in this way only 1D transport is relevant;
- "Sufficiently" low fin density on the surface;
- Perfect contact between the fin base and primary surface.

The full Pick and Sonnenberg [23] model accurately describes the hydrogen isotopes release from a surface, but requires the distinction between surface states and subsurface solute sites. Combining it with the work of Waelbroeck [22], it is possible to derive an effective recombination coefficient K_r that greatly simplifies the model. The applicability of the recombination coefficient to model the HI release depends on multiple assumptions [26] that are considered here reasonable taking into account that the problem is steady-state and analogous to a gas-driven permeation experiment. The low fin surface density assumption means that it is neglected the effect of a fin on the others.

The following analysis can be applied for both gas and liquid on the high pressure side. If a liquid–solid–gas is considered (PAV system, Hydrogen Permeation Sensors for liquid metals), the transport regime must be membrane limited [25], so the transport is independent of the features of the liquid domain, which is not considered in the analysis. However, this is also required from a performance point of view: if the regime is limited by mass transfer in the liquid, the finned surface approach is not beneficial.

In Fig. 1 the differential element of the fin is shown. The molar balance is expressed by:

$$\phi(x) - \phi(x+dx) = d\phi_r \tag{1}$$

where $\phi(x)$ (mol s^{-1}) and $\phi(x+dx)$ (mol s^{-1}) are the permeation rates at the relative coordinates and $d\phi_r$ (mol s^{-1}) is the differential recombination rate. This contributions are given by

$$\phi(x) = -A_c(x)\, D \frac{dc(x)}{dx} \tag{2}$$

$$\phi(x+dx) = -D\left(A_c(x)\frac{dc(x)}{dx} + \frac{d}{dx}\left(A_c(x)\frac{dc(x)}{dx}\right)dx\right) \tag{3}$$

$$d\phi_r = dA_l(x)\, K_r c(x)^2 = P(x)\, K_r c(x)^2\, dx \tag{4}$$

where $c(x)$ (mol m^{-3}) is the concentration of the chemical species, D (m^2 s^{-1}) is the diffusion coefficient, K_r (m^4 mol^{-1} s^{-1}) is the recombination coefficient and $P(x) = 2(w+\delta(x))$ (m) is the perimeter of the fin. Eq. (1) becomes:

$$D\frac{d}{dx}\left(A_c(x)\frac{dc(x)}{dx}\right)dx = P(x)\, K_r c(x)^2\, dx \tag{5}$$

and differentiating:

$$\frac{d^2c(x)}{dx^2} + \frac{1}{A_c(x)}\frac{dA_c(x)}{dx}\frac{dc(x)}{dx} = \frac{P(x)}{A_c(x)}\frac{K_r}{D}c(x)^2 \tag{6}$$

The molar balance can be simplified for the important case of a thin, straight fin with a rectangular cross-section. The latter assumption eliminates the dependence of the perimeter and the cross-sectional area on the coordinate x. For a rectangular fin, $P = 2(w+\delta)$ and $A_c = w\delta$. Furthermore, for a thin fin ($\delta \ll w$), their ratio is $P/A_c = 2(w+\delta)/w\delta \approx 2/\delta$. In this way, Eq. (6) takes this simple form:

$$\frac{d^2c(x)}{dx^2} = \frac{2}{\delta}\frac{K_r}{D}c(x)^2 \tag{7}$$

2.2. Solutions of the dimensionless model for a rectangular fin

The dimensionless concentration is defined as $c^*(x) = c(x)/(K_{s,s}\sqrt{p})$, where $K_{s,s}$ (mol m^{-3} $Pa^{-1/2}$) is the Sieverts' constant of the permeator and p (Pa) is the partial pressure of the hydrogen isotope on the left side of the membrane. The dimensionless geometrical parameters are weighted by the fin length l. Dividing by the steady-state, diffusion-limited permeation flux at the primary membrane with thickness t, expressed by $J = DK_{s,s}/t\sqrt{p}$ (mol m^{-2} s^{-1}), and introducing the dimensionless quantities, Eq. (7) becomes:

$$\frac{d^2c^*(x^*)}{dx^{*2}} = \frac{2}{\delta^* t^*} W c^*(x^*)^2 \tag{8}$$

where $W = K_r K_{s,s} t\sqrt{p}/D$ (-) is the permeation parameter related to the primary surface, x^* is the dimensionless coordinate and δ^* and t^* are the dimensionless geometric quantities. It is interesting to emphasise that the coefficient on the right-hand side includes the permeation parameter W, which depends only on the properties of the primary surface and driving pressure, and the geometrical quantities of the primary and secondary surfaces. It is here called W_f:

$$W_f = \frac{2W}{\delta^* t^*} = \frac{2\, W l^2}{\delta t} \tag{9}$$

Considering the assumptions of thin fin, $\delta \ll l$, and considering that, generally, $t \ll l$, the denominator is always less than one, thus $W_f > W$.

Eq. (8) is a second order nonlinear ordinary differential equation from the autonomous family [27]. It has the following general solution:

$$c^*(x^*) = \left(\frac{6}{W_f}\right)^{1/3} \wp\left(\left(\frac{W_f}{6}\right)^{1/3}(x^* + C_1); 0, C_2\right) \tag{10}$$

The function $\wp$ is the Weierstrass elliptic function and C_1, C_2 are integrating constants that can be found by introducing suitable boundary conditions. For the fin base, $x^* = 0$, the condition is $c^* = c_0^*$, where c_0^* is assumed to be known. The interesting case for fin application is when $W < 1$, and in this case $c_0^* \approx 1$, with better approximation when $W \ll 1$. To simplify the analysis, $c_0^* = 1$ is considered from now on. At the fin tip, $x^* = l^* = 1$, two bcs are examined:

- Long and thin fin ($\delta/l \approx 0$), for which $c^*(x^* = 1) = 0$;
- Thin fin with negligible permeation rate at the fin tip, for which $\frac{dc^*(x^*)}{dx^*}|_{x^*=1} = 0$.

The latter approximation is closest to the real problem, given that $\delta \ll l$, i.e., the permeation rate through the fin tip of area A_c is a small fraction of the total permeation rate of the secondary surface. The particular solutions for the two BCs are now obtained in the two extreme cases $W_f \ll 1$ and $W_f \gg 1$. When $W_f \ll 1$, Eq. (8) takes the simple form:

$$\frac{d^2c^*(x^*)}{dx^{*2}} = 0 \tag{11}$$

and the solutions, for the two set of boundary conditions are:

$$c^*(x^*) = (1 - x^*) \tag{12}$$

for the long and thin fin, and

$$c^*(x^*) = 1 \tag{13}$$

for the thin fin with impermeable tip.

To obtain the solution for the case $W_f \gg 1$, Laurent's series expansion of Eq. (10) can be carried out, which yields the following result:

$$c^*(x^*) \approx \frac{6}{W_f}\frac{1}{(x^* + c_1)^2} + \frac{W_f}{6}\frac{c_2}{28}(x^* + c_1)^4 \tag{14}$$

Introducing the boundary conditions, the following approximate solutions are obtained:

$$c^*(x^*) \approx \frac{6}{W_f\left(x^* + \sqrt{6/W_f}\right)^2}\left(1 - \left(\frac{x^* + \sqrt{6/W_f}}{1 + \sqrt{6/W_f}}\right)^6\right) \tag{15}$$

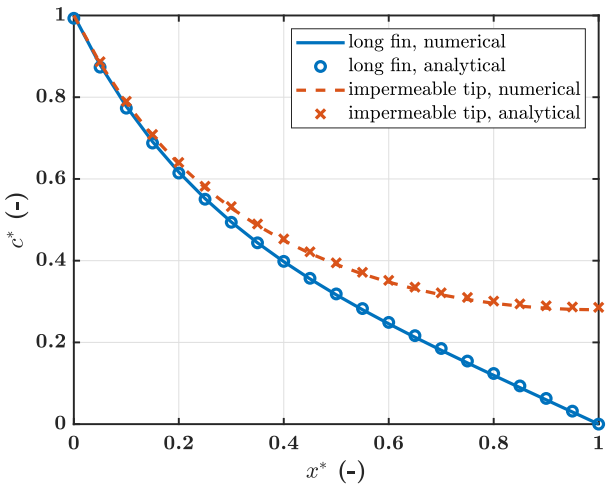

(a) $W_f = 10$.

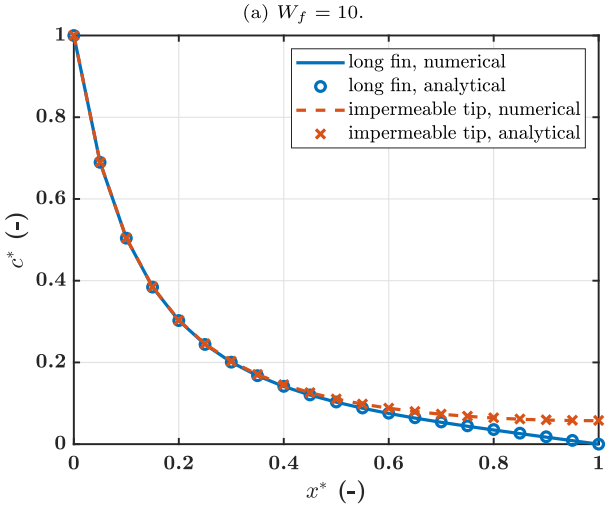

(b) $W_f = 100$.

Fig. 2. Analytical and numerical solutions comparison of the concentration $c^*(x^*)$.

for the long and thin fin, and

$$c^*\left(x^*\right) \approx \frac{6}{W_f\left(x^* + \sqrt{6/W_f}\right)^2}\left(1 + \frac{1}{2}\left(\frac{x^* + \sqrt{6/W_f}}{1 + \sqrt{6/W_f}}\right)^6\right) \tag{16}$$

for the thin fin with impermeable tip. In Fig. 2, the analytical solutions expressed by Eqs. (15) and (16) for $W_f = 10{,}100$ and $\delta^* = t^* = 0.05$ are compared to the numerical solution of Eq. (8) obtained integrating the differential equation with boundary conditions exploiting the *bvp4c* finite difference code in Matlab [28]. The resulting error, expressed as relative difference between the integrals of the $c(x)$ curves, that comes from the adoption of the approximate relation obtained for $W_f \gg 1$, decreases with the increase of W_f, going from 0.65% and 0.37% at $W_f = 10$ for the long fin and impermeable tip solutions, respectively, to 0.003% and 0.0035% at $W_f = 100$. The approximate solution still gives small errors even at $W_f = 10$.

2.3. Fin efficiency and effectiveness

The concept of fin efficiency is introduced, similar to the case of finned heat exchangers [29,30]. The permeation rate of the actual fin can be weighted by the permeation rate of a "perfect fin" that has same characteristics but diffusion coefficient $D \to \infty$, that leads to a constant concentration on the whole fin surface. Mathematically:

$$\eta_f = \frac{\phi_f}{\phi_{f,max}} \tag{17}$$

where η_f is the fin efficiency, ϕ_f is the permeation rate of the fin and $\phi_{f,max}$ is the permeation rate of the "perfect fin". Eq. (17) is expressed by:

$$\eta_f = \frac{A_l K_r \int_0^1 \left(c^*\left(x^*\right)\right)^2 dx^*}{A_l K_r c_0^{*2}} = \int_0^1 \left(c^*\left(x^*\right)\right)^2 dx^* \tag{18}$$

Given that $c_0^{*2} = 1$. Considering the solution of the concentration for $W_f \ll 1$ and long and thin fin, expressed by Eq. (12), and putting this value into the definition of efficiency:

$$\eta_f = \int_0^1 \left(1 - x^*\right)^2 dx^* = \frac{1}{3} \tag{19}$$

The fin efficiency for the fin with adiabatic tip can be obtained injecting (13) in the definition of η_f:

$$\eta_f = \int_0^1 1^2 dx^* = 1 \tag{20}$$

Thus, for small values of W_f, the fin becomes equivalent to the "perfect fin" and the efficiency takes the maximum value of 1.

In order to obtain an analytical expression for the efficiency at $W_f \gg 1$, it is necessary to evaluate the integral $\int_0^1 \left(c^*\left(x^*\right)\right)^2 dx^*$ where c^* is expressed by the relations (15) and (16). To reach the goal, it is easier to consider the general solution expressed by Eq. (10), and the integral can be expressed by:

$$\int_0^1 \left(\left(\frac{6}{W_f}\right)^{1/3} \wp\left(\left(\frac{W_f}{6}\right)^{1/3}\left(x^* + c_1\right); 0, c_2\right)\right)^2 dx^*$$
$$= \frac{1}{6}\left(\frac{6}{W_f}\right)^{1/3} \wp'\left(\left(\frac{W_f}{6}\right)^{1/3}\left(x^* + c_1\right); 0, c_2\right)$$

where $\wp'$ is the derivative with respect to x^* of the Weierstrass' elliptic function. Considering the Laurent's expansion of the derivative of $\wp$, and introducing the boundary conditions, the following relations can be derived:

$$\eta_f = \sqrt{\frac{2}{3W_f}}\left(1 - \left(\frac{\sqrt{6/W_f}}{1 + \sqrt{6/W_f}}\right)^3\right)\left(1 - 2\left(\frac{\sqrt{6/W_f}}{1 + \sqrt{6/W_f}}\right)^3\right) \tag{21}$$

for the long and thin fin, and

$$\eta_f = \sqrt{\frac{2}{3W_f}}\left(1 - \left(\frac{\sqrt{6/W_f}}{1 + \sqrt{6/W_f}}\right)^6\right) \tag{22}$$

for the impermeable fin. Eqs. (21) and (22) both take the same form considering that $\sqrt{6/W_f} \ll 1$:

$$\eta_f = \sqrt{\frac{2}{3W_f}} = \frac{1}{l}\sqrt{\frac{\delta t}{3W}} \tag{23}$$

The behaviour of fin efficiency as a function of $W_f = 2W/\delta^*/t^*$ is shown in Fig. 3, calculated for the two boundary conditions with the finite differences scheme *bvp4c*. The obtained analytical solutions overlap with the numerical solutions in the limits $W_f \ll 1$ and $W_f \gg 1$. As expected, the efficiency is highest for small values of W_f, which is typically the case for large diffusivity values, and decreases as the fin parameter increases. For high values of W_f, the two boundary conditions become equal. Finally, it is worth noting that the curves for the limiting cases agree with the exact solution of the equation even near $W_f = 1$. In particular, the solution for $W_f \ll 1$ overlaps with the exact solution at $W_f < 0.1$. The same applies to the solution for $W_f \gg 1$ at $W_f > 10$.

In Table 2, the summary of the analytical relations obtained for the fin efficiency η_f is presented.

A key parameter that can measure the fin performance is the fin effectiveness. It represents the gain in permeation rate due to the adoption of the secondary surface, being defined as the ratio between

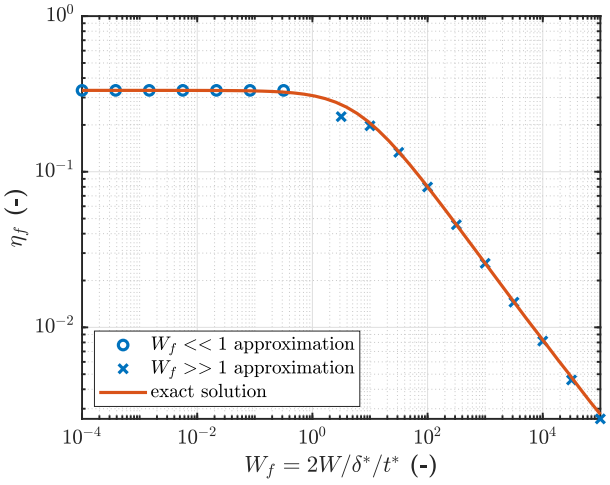

(a) Long fin.

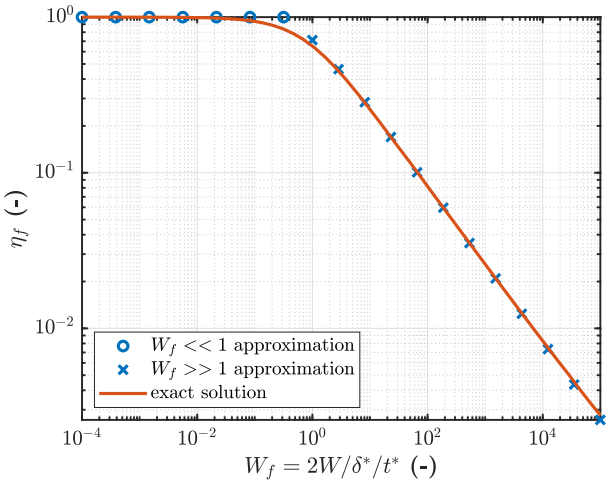

(b) Fin with impermeable tip.

Fig. 3. Fin efficiency as function of $W_f = 2W/\delta^*/t^*$ for a thin fin.

Table 2
Summary of the relations for η_f.

η_f	$W_f \ll 1$	$W_f \gg 1$
Long fin	$\frac{1}{3}$	$\frac{1}{l}\sqrt{\frac{\delta t}{3W}}$
Impermeable tip	1	$\frac{1}{l}\sqrt{\frac{\delta t}{3W}}$

the permeation rate of the fin and the permeation rate through the area of the primary surface covered by the fin, if the fin were removed ϕ_c:

$$\epsilon_f = \frac{\phi_f}{\phi_c} \tag{24}$$

Considering the definition, the fin effectiveness has to be $\epsilon_f > 1$ in order to get benefits from the adoption of secondary surfaces. Introducing the corresponding values, Eq. (24) becomes:

$$\epsilon_f = \frac{A_l K_r \int_0^1 (c^*(x^*))^2 \, dx^*}{A_c K_r c_0^{*2}} = \frac{2(w^* + \delta^*)}{w^* \delta^*} \eta_f \approx \frac{2}{\delta^*} \eta_f \tag{25}$$

Substituting the relations for η_f, Eqs. (19), (20) and (23) in the effectiveness definition, the analytical expressions for ϵ_f are obtained. For $W_f \ll 1$ and long fin:

$$\epsilon_f \approx \frac{2}{3\delta^*} = \frac{2l}{3\delta} \tag{26}$$

For $W_f \ll 1$ and impermeable tip:

$$\epsilon_f \approx \frac{2}{\delta^*} = \frac{2l}{\delta} \tag{27}$$

Table 3
Summary of the relations for ϵ_f.

ϵ_f	$W_f \ll 1$	$W_f \gg 1$
Long fin	$\frac{2l}{3\delta}$	$\sqrt{\frac{4t}{3\,W\delta}}$
Impermeable tip	$\frac{2l}{\delta}$	$\sqrt{\frac{4t}{3\,W\delta}}$

For both the bcs and $W_f \gg 1$:

$$\epsilon_f \approx \sqrt{\frac{4t^*}{3\,W\delta^*}} = \sqrt{\frac{4t}{3\,W\delta}} \tag{28}$$

In Table 3, the recap of the analytical relations obtained for the fin effectiveness ϵ_f is presented.

It is important to point out that although at $W_f \gg 1$ the fin efficiency η_f increases as δ increases, the fin effectiveness shows the opposite trend. It can be seen from the definition of fin effectiveness that reducing δ allows the cross-sectional area to decrease proportionally with little effect on the denominator terms, which instead depend on $sqrt(\delta)$. Reducing fin thickness has a beneficial effect on improving fin effectiveness. This behaviour is displayed also in Fig. 4(a), which shows η_f and ϵ_f as a function of $\delta^* = \delta/l$. Here the calculations were carried out numerically and the fin parameter takes values between 0.1 and 10, which covers the interval around $W_f = 1$.

Similar considerations can be made for the behaviour of η_f and ϵ_f when changing the dimensional fin length l. For $W_f \gg 1$ the efficiency is inversely proportional to l, as can be seen from Eq. (22) and from Fig. 4(b). For $W_f \ll 1$, the effectiveness increases linearly with the fin length, as can be seen from Eqs. (26) and (27), then, for $W_f \gg 1$ it becomes independent on l (Eq. (28)) and reaches an asymptote corresponding to the maximum performance of the fin in terms of permeation rate increase for given δ, t and transport properties. In this range, increasing the length of the fin provides progressively less benefit in terms of increasing the permeation rate. Based on the latter consideration, it is possible to define a relationship that can be used to select a first try value for the fin length. Substituting the definition of W_f into $W_f \gg 1$ yields:

$$l \gg \sqrt{\frac{\delta t}{2W}} \tag{29}$$

W_f is then particularly important in the design phase and allows the selection of the fin length that represents the best compromise between the increase in permeation rate and the size of the fin.

Figs. 5(a) and 5(b) show the 3D plots of fin efficiency and fin effectiveness as a function of δ^* and W for $t^* = 0.05$. ϵ_f is compared to the plane $f(\delta^*, W) = 1$. The latter divides the surface into two regions, one where the fin is advantageous, $\epsilon_f > 1$, and the other where it is disadvantageous. It is evident that for low values of the permeation parameter W, the use of secondary surfaces is highly beneficial to increase the permeation rate, with values of fin effectiveness even greater than 10^3. Also, for $W > 1$ there are δ^* that make $\epsilon_f > 1$, even considering permeation parameters of the order of thousands.

In the case where the concentration on the left side of the membrane is considered uniform (e.g. permeation sensors technology), it is possible to define a global performance parameter that takes into account the contributions of the entire primary and secondary surfaces. The overall fin effectiveness can be defined as the ratio between the permeation rate of the fin plus the remaining primary surface and the permeation rate of the primary surface if the fins were not present:

$$\epsilon_o = \frac{\phi_{p,max} + \phi_f}{\phi_{p,max,tot}} \tag{30}$$

where $\phi_{p,max,tot}$ is the permeation rate of the system without the fins. Manipulating and including the definition of ϵ_f, Eq. (30) reduces to:

$$\epsilon_o = 1 + \frac{A^*_{c,tot}}{A^*_{p,tot} + A^*_{c,tot}} (\epsilon_f - 1) \tag{31}$$

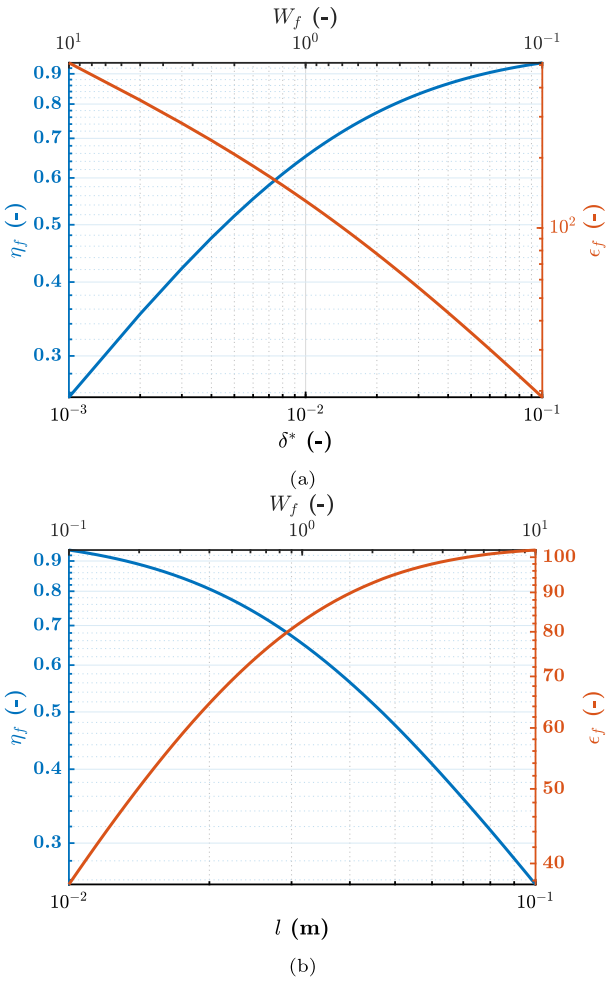

Fig. 4. Fin efficiency and fin effectiveness as a function of the non-dimensional fin thickness δ^* (top) and a function of the dimensional fin length l (bottom).

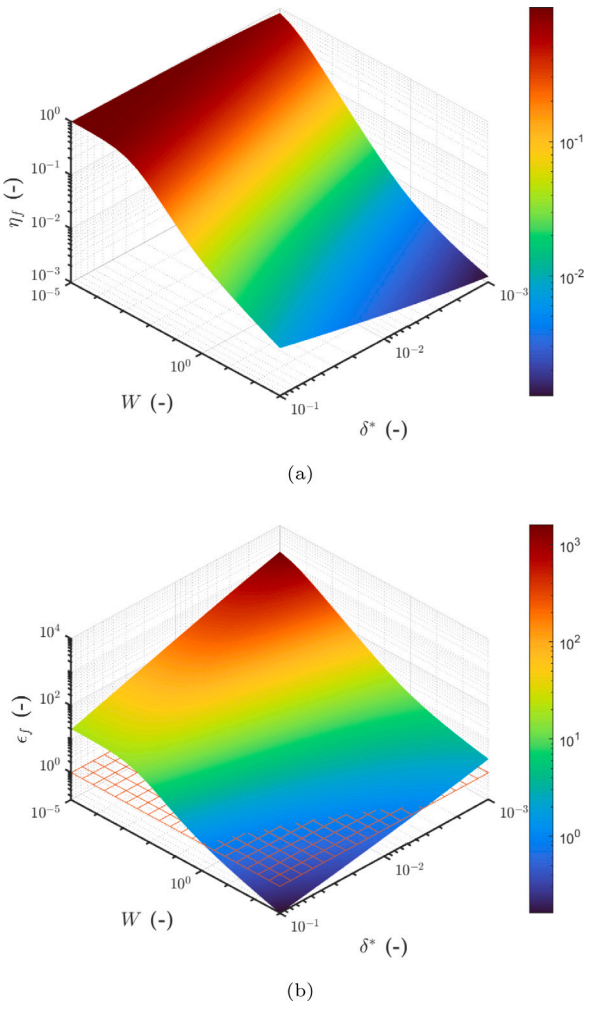

Fig. 5. Fin efficiency and fin effectiveness as a function of δ_f and W. For the bottom figure, the plane in red represents the breakeven value of $\epsilon_f = 1$.

Table 4
Summary of the relations for ϵ_o.

ϵ_o	$W_f \ll 1$	$W_f \gg 1$
Long fin	$1 + \frac{\delta n_f}{H}\left(\frac{2l}{3\delta} - 1\right)$	$1 + \frac{\delta n_f}{H}\left(\sqrt{\frac{4t}{3\,W\delta}} - 1\right)$
Impermeable tip	$1 + \frac{\delta n_f}{H}\left(\frac{2l}{\delta} - 1\right)$	$1 + \frac{\delta n_f}{H}\left(\sqrt{\frac{4t}{3\,W\delta}} - 1\right)$

Here $A^*_{c,tot}$ is the area of the primary surface covered by the fins. The ratio $A^*_{c,tot}/\left(A^*_{p,tot} + A^*_{c,tot}\right)$ is the fraction of the primary surface covered by the fins, and in the case of fins of equal size it is simply $A^*_{c,tot}/\left(A^*_{p,tot} + A^*_{c,tot}\right) = \delta n_f / H$, where n_f is the number of fins and H is the total height of the permeation membrane. The overall fin effectiveness can be maximised in the case $\epsilon_f > 1$ by increasing the factor $\delta n_f / H$, which corresponds to an increase of n_f for a fixed fin geometry. It should be pointed out that the analysis do not considers effects on the H concentration distribution due to the presence of adjacent fins. This interaction increases as the distance between the fins is reduced (increasing n_f). Table 4 reports a summary of the analytical relationships obtained for the fin effectiveness ϵ_o.

The practical usefulness of the overall effectiveness of the fins is simple: once the properties of the membrane and thus the theoretical permeation rate are defined, the permeation rate of a finned configuration can be predicted by multiplying this value by the overall effectiveness, after defining the number and geometry of the secondary surfaces. Recall that the best increase in performance occurs after the introduction of secondary surfaces when $W \ll 1$ and $W_f \gg 1$.

3. Extended surface application

A numerical analysis is now reported to characterise the performance of a permeator with the features of a typical Permeator Against Vacuum system [10–13,20,31]. In particular, a $t = 0.5$ mm niobium slab maintained at 500 °C was considered. On the left, a eutectic lithium-lead alloy in thermal equilibrium with the membrane carries monoatomically dissolved tritium with a concentration of $1.41 \cdot 10^{-2}$ mol m^{-3}, which is the expected value at the inlet of the extractor of a D-T fusion reactor [32]. According to Sieverts' law and the assumption of Aiello's solubility constant $K_{s,PbLi} = 2.37 \cdot 10^{-1} \exp\left(-1.28 \cdot 10^4 / R/T\right)$ [33], the tritium partial pressure corresponds to $1.93 \cdot 10^{-1}$ Pa. Tritium then moves through the Nb membrane with a diffusivity D_{Nb} adopted from Alefeld and Voelkl [34], which was divided by the coefficient $\sqrt{3}$ to account for the fact that tritium and not protium is considered. The solubility $K_{s,Nb}$ of Veleckis and Edwards [35] has been adopted. The hydrogen isotope is then released from the surface where it recombines in diatomic form. The constant for this process, $K_{r,Nb}$, has been taken from Pick and Sonnenberg [23], for two conditions, a clean surface and an oxidised surface. In the first case, the permeation parameter is $W = 7.09 \cdot 10^{-1}$, while for the oxidised

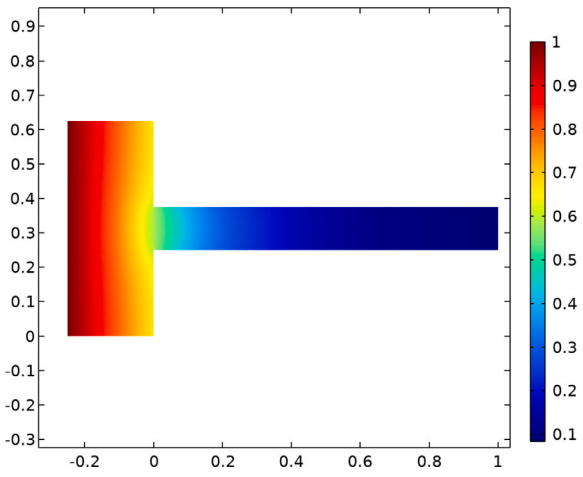

Fig. 6. Dimensionless concentration profile of a particular solution of the domain considered in the 2D numerical analysis.

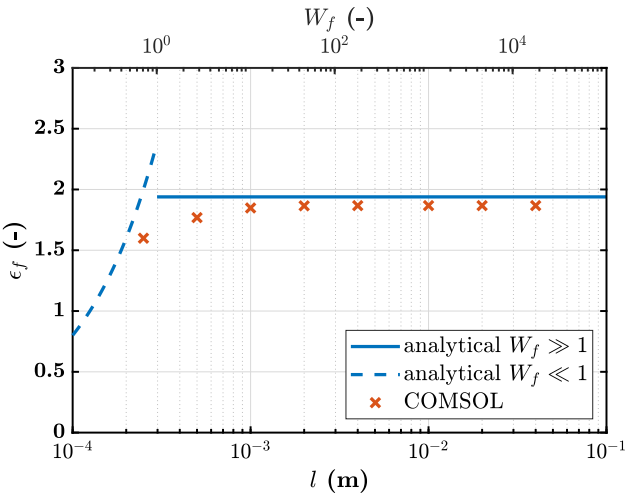

Fig. 7. Fin effectiveness as a function of the dimensional fin length l for a clean surface.

surface $W = 9.53 \cdot 10^{-5}$. The fin thickness considered in all the following analyses is $\delta = 0.25$ mm.

It has been seen experimentally that under certain conditions mass transport in the liquid can be the factor that limits hydrogen extraction in PAV systems [13]. This can reduce the usefulness of the fins, especially if the surfaces can be maintained clean. Nevertheless, strategies to improve the mass transfer in the liquid can be applied (e.g. improving mixing), shifting the transport regime to membrane-limited. In the current analysis the regime is assumed to be membrane limited [25], therefore the liquid region is not considered in this analysis and a constant value of the concentration on the left side of the membrane is assumed, equating the partial pressures at the liquid/solid interface. This is not a bold assumption for the oxidised membrane case, where the very low permeation parameter almost ensures a surface-limited regime. In this case, positive effects are expected from the use of secondary surfaces. To further simplify the analysis, the width of the system is considered larger than the other dimensions, simplifying the geometry to 2D. In addition, the gradient of tritium concentration in the direction of motion of the fluid, y, is neglected. In this way, only one fin and half of the two adjacent non-finned surfaces are simulated. The steady-state transport equation is solved in the solid domain using the mHIT code [36] developed with COMSOL Multiphysics:

$$-D\nabla^2 c = 0 \tag{32}$$

The following boundary conditions are considered: at the left side of the membrane, a constant value of concentration has been imposed

$$c = K_{s,Nb}\sqrt{p} \tag{33}$$

and at the solid–gas interface:

$$\vec{J} \cdot \hat{n} = -K_{r,Nb}c^2 \tag{34}$$

where $\hat{n}$ is the unitary vector normal to the surface. The problem is solved in dimensionless form, keeping the strategy from the previous section. In Fig. 6, the domain showing a concentration profile along the finned geometry is represented.

The permeation rates, expressed in mol s^{-1}, are calculated for both the non-finned and the finned membranes. The ratio between the permeation rate of the finned surface and the finned base in the non-finned case corresponds, by definition, to the fin effectiveness ϵ_f. The numerical value is compared with the analytical value obtained from the simplified relations Eqs. (27) and (28). The results are shown in Figs. 7 and 8, with a sensitivity study on the change in fin length l.

In Fig. 7 the results for a clean surface are shown. The permeation parameter W is about 1, so no great advantage is expected from the introduction of the fins. Nevertheless, the increase in permeation rate due to the use of secondary surfaces is not negligible and goes from 60% to >%85 for a fin of length $l > t$. For small l, the analytical expression overestimates the effectiveness of the fins. This is due to two factors: W_f is about 1, so the two limiting solutions obtained for $W_f \ll 1$ and $W_f \gg 1$ are not applicable. In addition, the fin length is close to the fin thickness, so that the assumption $l \gg \delta$ is not fulfilled. However, for the smallest value of l, the difference between the two solutions is around 20% and decreases to less than 4% for $l = 4\delta$ or larger. It is interesting to see that for $W_f > 10$ there are no additional benefits when fin length is increased, confirming the results from Section 2.

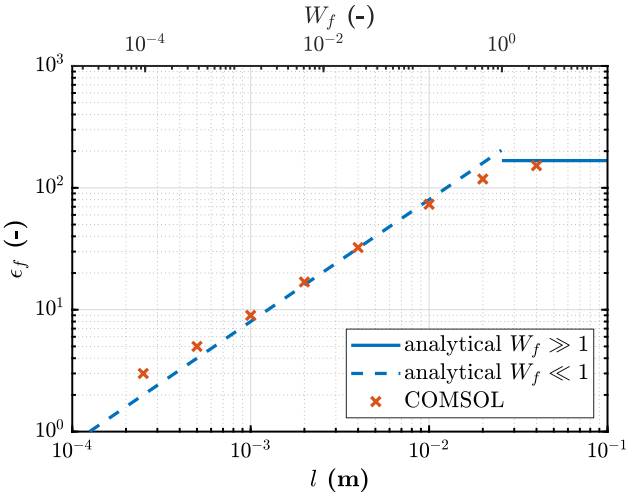

Fig. 8. Fin effectiveness as a function of the dimensional fin length l for a oxidised surface.

In Fig. 8 the results for the oxidised surface are shown. In this case, the permeation parameter is below $1 \cdot 10^{-4}$, and the effectiveness increases from $\epsilon_f = 3$ for the very small fin length $l = 0.25$ mm (length equal to the fin thickness δ) to $\epsilon_f > 100$ at $l = 20$ mm. For these values W_f is still well below 1, so it will be possible to increase the fin length with positive effects. An important point here is that the volume of the finned membrane is 8 times that of the unfinned one, while the ϵ_f is 118, due to the increased surface area of 160 times. It must be pointed out that, although an increase in volume will determine an increase in tritium inventory in the system and longer times to reach steady-state, the gain in terms of permeation rate obtained using a

secondary surface can be extremely higher. At $l = 40$ mm (last point), $W_f \sim 15$ and the numerical solution is consistent with the analytical solution for $W_f \gg 1$, the area in which increasing the length of the fin starts to be less effective. As for the comparison between the two solutions, the difference between the analytical and numerical solutions is not negligible for small l and is about 30%, while it is about 1% for intermediate values where $W_f \ll 1$ and $l \gg \delta$.

4. Discussion

It has been shown that secondary surfaces placed on the vacuum side can be used with great advantages when the regime is surface-dominating or surface-limited, attaining great increases in terms of tritium permeation rate with small increase in membrane material. In this framework, $W_f = 2Wl^2/\delta/t$ represents an important design parameter. In fact, in the regions where the adoption of secondary surfaces is beneficial, $\epsilon_f > 1$, the highest achievable permeation rate has been shown to correspond to the region $W_f \gg 1$, where fin effectiveness approaches a horizontal asymptote and an increase in fin length starts to have a smaller impact on permeation rate improvement. From W_f we get the relationship $l \gg \sqrt{\delta t/2/W}$, which provides a first try value for the choice of fin length. It has been shown that even small fins can be advantageous ($l \approx \delta$), with limited manufacturing complexity. In addition, a strategy can be also to apply fins just to certain portions of the extraction system, where the tritium partial pressure is low (lower W) and where their effectiveness is higher. Compared to the heat transfer case, the presence of secondary surfaces does not have the disadvantage of increasing the pressure drop, as the secondary surfaces are on the vacuum side, but the fins can have an effect on the conductance of the vacuum system, especially in the case of internally finned permeators where the characteristic length of the system is particularly small. The use of fins increases the volume of the system therefore the inventory and the time required to reach steady-state operation, but can lead to much bigger permeation rates.

Among the assumptions considered in the analysis, some need special attention. In tritium permeation systems, it is possible to have the presence of multiple hydrogen isotopes, and this was not included in the analysis. In order to apply the relations here attained, it is important to check if the presence of different isotopes has an impact on the permeation kinetics. Negligible pressure on the vacuum side was assumed. The impact of non-null pressure on the vacuum side cannot be addressed by the equations derived, but having a low pressure on the vacuum side (compared to the tritium partial pressures in the liquid and membrane) is a design requirement in order to maximise the performances of the permeator. Perfect contact between the base of the fin and the primary surface was assumed. This needs to be further investigated considering the manufacturing methods of the permeation system, that could be comparable to the one used for heat exchanger systems. Lastly, the mutual interaction of the fins has still to be investigated.

CRediT authorship contribution statement

Ciro Alberghi: Writing – review & editing, Writing – original draft, Software, Methodology, Investigation, Formal analysis, Conceptualization. **Luigi Candido:** Writing – review & editing, Investigation. **Daniele Martelli:** Writing – review & editing, Supervision. **Francesca Papa:** Writing – review & editing. **Marco Utili:** Writing – review & editing, Supervision. **Alessandro Venturini:** Writing – review & editing.

Declaration of competing interest

The authors declare that they have no known competing financial interests or personal relationships that could have appeared to influence the work reported in this paper.

Acknowledgements

This work has been carried out within the framework of the EUROfusion Consortium, funded by the European Union via the Euratom Research and Training Programme (Grant Agreement No 101052200 — EUROfusion). Views and opinions expressed are however those of the author(s) only and do not necessarily reflect those of the European Union or the European Commission. Neither the European Union nor the European Commission can be held responsible for them.

Data availability

Data will be made available on request.

References

[1] A. Ciampichetti, M. Zucchetti, I. Ricapito, M. Utili, A. Aiello, G. Benamati, Performance of a hydrogen sensor in Pb–16Li, J. Nucl. Mater. 367–370 (2007) 1090–1095, http://dx.doi.org/10.1016/j.jnucmat.2007.03.250.
[2] I. Nicolotti, M. Utili, L. Candido, M. Zucchetti, A hydrogen sensor for liquid-metal breeding blankets, Trans. Am. Nucl. Soc. 112 (2015) 193–196.
[3] L. Candido, I. Nicolotti, M. Utili, M. Zucchetti, Design optimization of a hydrogen sensor for ITER Pb16Li blankets, IEEE Trans. Plasma Sci. 45 (7) (2017) 1831–1836, http://dx.doi.org/10.1109/TPS.2017.2710218.
[4] L. Candido, et al., HyPer-QuarCh II: A laboratory-scale device for hydrogen isotopes permeation experiments, Fusion Eng. Des. 172 (2021) 112920, http://dx.doi.org/10.1016/j.fusengdes.2021.112920.
[5] L. Candido, M. Cantore, E. Galli, R. Testoni, M. Zucchetti, M. Utili, A. Ciampichetti, Characterization of pb-15.7li hydrogen isotopes permeation sensors and upgrade of hyper-quarch experimental device, IEEE Trans. Plasma Sci. 48 (6) (2020) 1505–1511, http://dx.doi.org/10.1109/TPS.2020.2974937.
[6] M. Utili, C. Alberghi, L. Candido, F. Papa, M. Tarantino, A. Venturini, TRIEX-II: An experimental facility for the characterization of the tritium extraction unit of the WCLL blanket of ITER and DEMO fusion reactors, Nucl. Fusion 62 (2022) 066036, http://dx.doi.org/10.1088/1741-4326/ac5c74.
[7] B. Garcinuno, et al., The CIEMAT LiPb loop permeation experiment, Fusion Eng. Des. 146 (2019) 1228–1232, http://dx.doi.org/10.1016/j.fusengdes.2019.02.045.
[8] C.N. Taylor, T.F. Fuerst, R.J. Pawelko, M. Shimada, The tritium extraction experiment (TEX): A forced convection fusion blanket PbLi loop, Fusion Eng. Des. 192 (2023) 113737, http://dx.doi.org/10.1016/j.fusengdes.2023.113737.
[9] K. Jiang, et al., Development of the high temperature PbLi experimental facility for CFETR, Fusion Eng. Des. 202 (2024) 114313, http://dx.doi.org/10.1016/j.fusengdes.2024.114313.
[10] F. Papa, et al., Engineering design of a permeator against vacuum mock-up with niobium membrane, Fusion Eng. Des. 166 (2021) 112313, http://dx.doi.org/10.1016/j.fusengdes.2021.112313.
[11] F. Papa, et al., Manufacturing of PAV-ONE, a permeator against vacuum mock-up with niobium membrane, Energies 16 (2023) 5471, http://dx.doi.org/10.3390/en16145471.
[12] F. Papa, A. Venturini, D. Martelli, M. Utili, Tritium extraction from lithium–lead eutectic alloy: Experimental characterization of a permeator against vacuum mock-up at 450 °C, Energies 16 (2023) 3022, http://dx.doi.org/10.3390/en16073022.
[13] A. Venturini, F. Papa, C. Alberghi, D. Martelli, M. Utili, Testing of PAV-ONE, a permeator against vacuum mock-up with niobium membrane, in lithium-lead eutectic at 350 °C, Fusion Eng. Des. 200 (6) (2024) 114215, http://dx.doi.org/10.1016/j.fusengdes.2024.114215.
[14] B. Garcinuño, D. Rapisarda, I. Fernández-Berceruelo, D. Jiménez-Rey, J. Sanz, C. Moreno, I. Palermo, Á. Ibarra, Design and fabrication of a permeator against vacuum prototype for small scale testing at lead-lithium facility, Fusion Eng. Des. 124 (2017) 871–875, http://dx.doi.org/10.1016/j.fusengdes.2017.02.060.
[15] T.F. Fuerst, C.N. Taylor, P.W. Humrickhouse, The source permeator system and tritium transport in the TEX PbLi loop, Fusion Sci. Technol. 79 (2022) 1–18, http://dx.doi.org/10.1080/15361055.2022.2090784.
[16] T.F. Fuerst, M.D. Eklund, J.A. Leland, A.A. Riet, C.N. Taylor, Parametric study of the vacuum permeator for the tritium extraction experiment, Fusion Sci. Technol. 79 (2023) 1–11, http://dx.doi.org/10.1080/15361055.2023.2196237.
[17] F. Okino, P. Calderoni, R. Kasada, S. Konishi, Feasibility analysis of vacuum sieve tray for tritium extraction in the HCLL test blanket system, Fusion Eng. Des. 109–111 (2016) 1748–1753, http://dx.doi.org/10.1016/j.fusengdes.2015.10.004.
[18] F.R. Urgorri, et al., Theoretical evaluation of the tritium extraction from liquid metal flows through a free surface and through a permeable membrane, Nucl. Fusion 63 (2023) 046025, http://dx.doi.org/10.1088/1741-4326/acbec7.
[19] G. Federici, L. Boccaccini, F. Cismondi, M. Gasparotto, Y. Poitevin, I. Ricapito, An overview of the EU breeding blanket design strategy as an integral part of the DEMO design effort, Fusion Eng. Des. 141 (2019) 30–42, http://dx.doi.org/10.1016/j.fusengdes.2019.01.141.

[20] A. Venturini, et al., Progresses in developing the Tritium Extraction and Removal system for the Water-Cooled Lithium-Lead Breeding Blanket in EUROfusion, Fusion Eng. Des. Under review.
[21] I. Ali-Khan, K. Dietz, F. Waelbroeck, P. Wienhold, The rate of hydrogen release out of clean metallic surfaces, J. Nucl. Mater. 76–77 (1978) 337–343, http://dx.doi.org/10.1016/0022-3115(78)90167-8.
[22] F. Waelbroeck, et al., Influence of Bulk and Surface Phenomena on the Hydrogen Permeation Through Metals, Tech. Rep. KFA Report JUL-1966, Forschungszentrum Julich Germany, 1984.
[23] M.A. Pick, K. Sonnenberg, A model for atomic hydrogen-metal interactions — application to recycling, recombination and permeation, J. Nucl. Mater. 131 (1985) 208–220, http://dx.doi.org/10.1016/0022-3115(85)90459-3.
[24] P.W. Humrickhouse, B.J. Merrill, Vacuum permeator analysis for extraction of tritium from DCLL blankets, Fusion Sci. Technol. 68 (2015) 295–302, http://dx.doi.org/10.13182/FST14-941.
[25] C. Alberghi, L. Candido, M. Utili, M. Zucchetti, Development of new analytical tools for tritium transport modelling, Fusion Eng. Des. 177 (2022) 113083, http://dx.doi.org/10.1016/j.fusengdes.2022.113083.
[26] K. Schmid, M. Zibrov, On the use of recombination rate coefficients in hydrogen transport calculations, Nucl. Fusion 61 (2021) 086008, http://dx.doi.org/10.1088/1741-4326/ac07b2.
[27] A.D. Polyanin, V.F. Zaitsev, Handbook of Exact Solutions for Ordinary Differential Equations, Chapman & Hall/CRC, 2003, http://dx.doi.org/10.1201/9781315117638.
[28] J. Kierzenka, L.F. Shampine, A BVP solver based on residual control and the matlab PSE, ACM Trans. Math. Software 27 (2009) 299–316, http://dx.doi.org/10.1145/502800.502801.
[29] B.S.V. Prasad, Fin efficiency and mechanisms of heat exchange through fins in multi-stream plate-fin heat exchangers: formulation, Int. J. Heat Mass Transfer 39 (1996) 419–428, http://dx.doi.org/10.1016/S0017-9310(97)80962-3.
[30] R.K. Shah, D.P. Sekulic, Fundamentals of Heat Exchangers Design, Wiley, 2003, http://dx.doi.org/10.1002/9780470172605.
[31] M. Utili, C. Alberghi, et al., Design and integration of the WCLL tritium extraction and removal system into the European DEMO tokamak reactor, Energies 16 (2023) 5231, http://dx.doi.org/10.3390/en16135231.
[32] L. Candido, et al., Design Advanced TERS and Upgrade TRIEX-II Vacuum System, Tech. Rep. BB-6.3.5-T001-D002, EUROfusion, 2020.
[33] A. Aiello, A. Ciampichetti, G. Benamati, Determination of hydrogen solubility in lead lithium using SOLE device, Fusion Eng. Des. 81 (2006) 639–644, http://dx.doi.org/10.1016/j.fusengdes.2005.06.364.
[34] G. Alefeld, J. Voelkl, Hydrogen in Metals I, vol. 1, Springer-Verlag, 1978, p. 321, http://dx.doi.org/10.1007/3-540-08705-2.
[35] E. Veleckis, R.K. Edwards, Thermodynamic properties in the systems vanadium-hydrogen, niobium-hydrogen, and tantalum-hydrogen, J. Phys. Chem. 73 (1969) 683–692, http://dx.doi.org/10.1021/j100723a033.
[36] L. Candido, C. Alberghi, Verification and validation of mHIT code over TMAP for hydrogen isotopes transport studies in fusion-relevant environments, Fusion Eng. Des. 172 (2021) http://dx.doi.org/10.1016/j.fusengdes.2021.112740.